An RNA guanine quadruplex regulated pathway to TRAIL-sensitization by DDX21

EWAN K.S. MCRAE,[1] STEVEN J. DUPAS,[1] EVAN P. BOOY,[1] RAMANAGURU S. PIRAGASAM,[2] RICHARD P. FAHLMAN,[2,3] and SEAN A. MCKENNA[1,4]

[1]Department of Chemistry, University of Manitoba, Winnipeg, Manitoba, Canada R3T 2N2
[2]Department of Biochemistry, University of Alberta, Edmonton, Alberta, Canada T6G 2H7
[3]Department of Oncology, University of Alberta, Edmonton, Alberta, Canada T6G 2R7
[4]Department of Biochemistry and Medical Genetics, University of Manitoba, Winnipeg, Manitoba, Canada R3E 0J9

ABSTRACT

DDX21 is a newly discovered RNA G-quadruplex (rG4) binding protein with no known biological rG4 targets. In this study we used label-free proteomic MS/MS to identify 26 proteins that are expressed at significantly different levels in cells expressing an rG4-binding deficient DDX21 (M4). MS data are available via ProteomeXchange with identifier PXD013501. From this list we validate MAGED2 as a protein that is regulated by DDX21 through rG4 in its 5′-UTR. MAGED2 protein levels, but not mRNA levels, are reduced by half in cells expressing DDX21 M4. MAGED2 has a repressive effect on TRAIL-R2 expression that is relieved under these conditions, resulting in elevated TRAIL-R2 mRNA and protein in MCF-7 cells, rendering them sensitive to TRAIL-mediated apoptosis. Our work identifies the role of DDX21 in regulation at the translational level through biologically relevant rG4 and shows that MAGED2 protein levels are regulated, at least in part, by the potential to form rG4 in their 5′-UTRs.

Keywords: DDX21; RNA; quadruplex; MAGED2; TRAIL-R2; proteomics

INTRODUCTION

DDX21 is an RNA helicase with a diverse set of biological functions. It plays important roles in ribosomal RNA biogenesis (Henning et al. 2003; Yang et al. 2003) by coordinating Pol I transcription and association of late acting snoRNAs with preribosomal complexes (Calo et al. 2014; Sloan et al. 2015). DDX21 has also been implicated in double-stranded RNA sensing and antiviral response (Zhang et al. 2011; Chen et al. 2014; Dong et al. 2016; Hammond et al. 2018) as well as epigenetic silencing of genes (Zhang et al. 2018). Abnormal levels of DDX21 protein has been observed in colorectal (Jung et al. 2011) and breast cancers (Cimino et al. 2008), where it has been correlated with disease-free survival, possibly mediated by regulating c-Jun activity and rRNA biogenesis (Holmström et al. 2008; Zhang et al. 2014). Recently, we have shown that DDX21 can bind and unwind RNA guanine-quadruplexes (rG4s) and affect the translation of a reporter construct with a rG4 in its 5′ untranslated region (UTR) of its mRNA (McRae et al. 2017). This activity is mediated by an evolutionarily conserved repeat region (F/PRGQR) in its carboxyl terminus that preferentially interacts with the backbone of rG4s (McRae et al. 2018). Recently, individual-nucleotide resolution cross-linking and immunoprecipitation (iCLIP) data using anti-DDX21 antibodies showed that ~35% of DDX21-bound RNA is mRNA (Calo et al. 2018), yet rG4 targets of DDX21 in mRNA have not been explored.

rG4s are four-stranded RNA structures that form in guanine-rich regions. When four guanines align in a plane they can form an extended hydrogen-bonding network called a guanine tetrad. Successive guanine tetrads can pi stack on top of one another to form a stable rG4 structure. The canonical rG4 forming sequence is $GGG(N_{1-7})GGG(N_{1-7})GGG(N_{1-7})GGG$, where (N_{1-7}) represents a short loop of 1–7 nt. However, longer loops as well as interrupted G-tracts have been shown to allow for rG4 formation. Canonical rG4s (Bugaut and Balasubramanian 2012) as well as noncanonical rG4s (Bolduc et al. 2016) present in mRNA have been shown to modulate mRNA translation

through stalling of scanning preinitiation complexes on 5′-UTRs (Bugaut and Balasubramanian 2012), by impacting alternative splicing (Ribeiro et al. 2014; Huang et al. 2017; Weldon et al. 2018), or through affecting miRNA binding to 3′-UTRs (Booy et al. 2014; Rouleau et al. 2017). A transcriptome-wide sequencing approach that exploits the ability of RNA rG4s to cause reverse transcriptase stop (rG4-seq) has identified thousands of rG4, many of which are noncanonical rG4s that would likely be missed by bioinformatic searches (Kwok et al. 2016). A major source of rG4 resolving activity (Creacy et al. 2008), DHX36, has been shown to bind multiple G-rich mRNA targets and DHX36 knockout renders these mRNA translationally incompetent (Sauer et al. 2019). Multiple rG4-containing mRNA targets of DHX36 have been identified and a mechanism proposed whereby it regulates translation by resolving rG4s (Chen et al. 2018). If not resolved these rG4s can lead to translation initiation at upstream open reading frames, precluding the translation of the downstream open reading frame (Murat et al. 2018). This work also showed DDX21 to be highly abundant at translationally active polysome fractions but did not investigate its role in rG4 mediated translational regulation.

In our current study, we use proteomic mass spectrometry (MS) to compare the levels of proteins in cell populations that are expressing wild-type DDX21 or a DDX21 mutant with impaired rG4 binding and unwinding abilities but intact duplex unwinding (DDX21 M4) (Valdez 2000; Valdez et al. 1997; McRae et al. 2017). We compare this list of candidate proteins to an rG4-seq database (Kwok et al. 2016), revealing a significant enrichment for rG4-containing mRNA in our list of candidate proteins. We then confirm the interaction of DDX21 with the mRNA of some candidate proteins by immunoprecipitation of DDX21 and quantitative PCR on bound RNA (RIP-qPCR).

The abundance of a promising candidate protein, Melanoma associated antigen D2 (MAGED2) protein, is significantly reduced in cells expressing DDX21 M4 in place of the wild-type helicase. MAGE proteins are a diverse set of proteins that contain the MAGE homology domain (MHD); the majority of the MAGE family of proteins are tumor antigens (Xiao and Chen 2005). An exception to this is the MAGED family; these proteins are expressed ubiquitously and contain none of the 20 antigenic peptides known to be recognized by T-lymphocytes (Lucas et al. 1999). MAGED proteins are known to regulate cell cycle progression, apoptosis, and transcription and are upregulated in key points of embryogenesis as well as in multiple cancer types (Kurt et al. 2000; Barker and Salehi 2002).

Overexpression of MAGED2 has been implicated in cancer progression and resistance to treatment of human breast cancers, specifically, MAGED2 acts as a transcriptional repressor of tumor necrosis factor-related apoptosis-inducing ligand (TRAIL) death receptor 2 (TRAIL-R2) mRNA (Tseng et al. 2012; Strekalova et al. 2016). TRAIL

has long been studied as a natural antitumoral protein with the ability to selectively trigger cell death in cancer cells through interactions with surface-expressed receptors, DR4 and DR5 (TRAIL-R1 and TRAIL-R2) (Mérino et al. 2007). TRAIL resistance occurs in breast cancer cells when the death receptors DR4 and TRAIL-R2 are no longer expressed on the cell surface (Zhang and Zhang 2008). TRAIL sensitization is emerging as a novel therapeutic target for treating resistant breast cancers by increasing TRAIL-R2 expression and then treating with TRAIL (Trivedi and Mishra 2015; Manouchehri et al. 2018). We confirm by qPCR and western blot that regulation of MAGED2 by DDX21 also affects the downstream target of MAGED2, TRAIL-R2, and imparts sensitivity to TRAIL-mediated apoptosis in a model breast cancer cell line (MCF-7).

To further investigate the link between rG4 and MAGED2 we synthesized a mutant version of the MAGED2 5′-UTR with G to C mutations that disrupt rG4 formation. We provide direct evidence of rG4 formation in the in vitro transcribed wild-type 5′-UTR but not the mutant UTR by using an RNA G4 specific fluorescent probe, Thioflavin T (ThT), and a modified reverse transcription stop method that also demonstrates rG4 unwinding by DDX21 in vitro. A side-by-side comparison of the effect of wild-type and mutant 5′-UTR in a luciferase assay reveals a loss of DDX21-mediated regulatory effect when rG4 are not present in the 5′-UTR. Together these results indicate that DDX21 regulates translation of MAGED2 mRNA in an rG4 dependent manner and contributes to the sensitization to TRAIL-mediated apoptosis.

RESULTS

Identifying putative rG4 targets of DDX21

To look for potential rG4 targets of DDX21 we wanted to compare cell populations expressing wild-type DDX21 versus a mutant DDX21 that has impaired rG4 binding and unwinding activities (M4). The M4 mutant contains a PRGQR to YEGIQ mutation in the carboxy-terminal repeat region of DDX21 that has been previously shown to disrupt rG4 binding and unwinding activities (McRae et al. 2017). Previous studies have also shown that deletion of the entire carboxy-terminal 209 amino acids results in only a 25% decrease in dsRNA helicase activity, while completely abolishing rG4 helicase activity (Valdez et al. 1997), indicating that the M4 mutation should not significantly affect non-rG4 structures. Differences observed between the wild-type DDX21 recovery (WT) and M4 DDX21 recovery experiments are therefore primarily due to differences in DDX21–rG4 interactions.
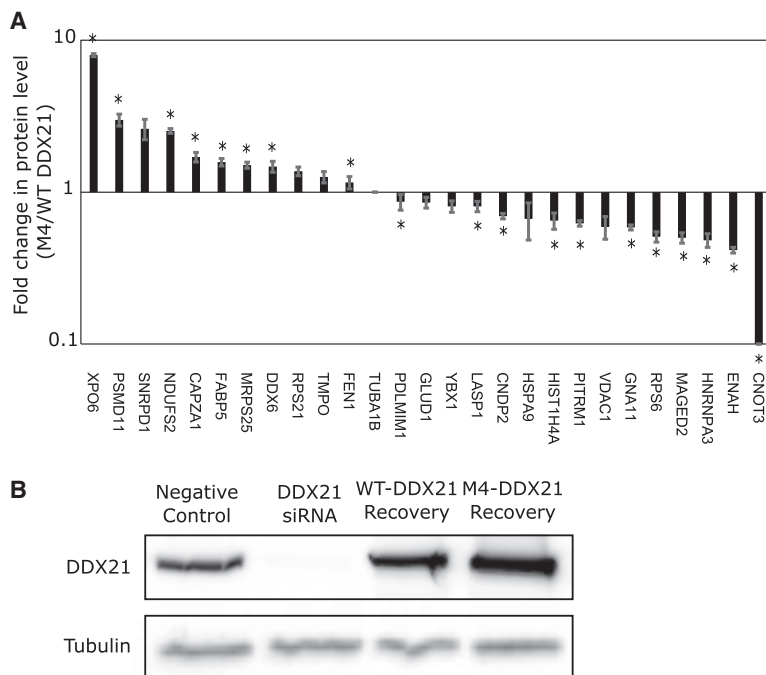
Briefly, HEK293T cells were first transfected with a plasmid expressing either WT or M4 DDX21. Following this, endogenous DDX21 was depleted by siRNA knockdown. Using label-free whole-cell proteome analysis we

identified 26 candidate proteins (Fig. 1A) whose expression level was significantly different between the M4 and WT samples. The data in Figure 1A is represented as the ratio of the amount of a protein detected in the M4 versus WT samples, this allows us to visualize a fold change in protein level in the absence of DDX21's rG4-binding activity. Proteins with values below 1 were detected in decreased abundance in the presence of M4 DDX21, indicating that the rG4 may be impeding protein expression. Proteins with values above 1 have increased abundance in the presence of M4 DDX21, indicating that a rG4 could be promoting expression of the protein; such mechanisms could include IRES formation or ribosome shunting (Rogers et al. 2004; Morris et al. 2010).

The efficiency of endogenous DDX21 knockdown was confirmed by MS where DDX21 was undetected in two of three knockdown samples and 10-fold less than negative control in the third replicate. The exogenous DDX21 (WT and M4) from the recovery samples was on average 10-fold more abundant than the endogenous DDX21 present in negative control samples. In order to exclude any artefactual differences caused by overexpression of the wild-type protein, proteins that were significantly different between our negative control (NC), which expresses only endogenous DDX21, and WT recovery sample groups were excluded. Any proteins that were not significantly different between NC and M4 recovery sample groups were also excluded. The efficiency of knockdown and recovery of DDX21 was also assessed by western blot (Fig. 1B).

From the list of 26 candidate proteins, 19 (73%) were shown to have quadruplex forming regions in their mRNA by rG4-seq experiments (Kwok et al. 2016). Comparatively, of the 17,622 unique transcripts mapped in the rG4-seq experiment only 37.5% showed evidence of RNA rG4 formation. The average rG4 density per kilobase of mRNA has previously been reported as 0.1, 0.02, and 0.08 rG4/kb for the 5′-UTR, coding sequence (CDS) and 3′-UTR, respectively (Kwok et al. 2016). The rG4 density observed in the mRNA of our candidate proteins was determined to be 0.8, 0.09, and 0.2 rG4/kb for 5′-UTR, CDS and 3′-UTR regions. Statistical significance of the enrichment of our 26 candidate proteins for rG4 formation was confirmed by Fisher's exact test, which yields a *P*-value of <0.0001 at a 99% confidence interval. Of the 19 candidate proteins shown to have rG4 in their mRNA, 45% were in the 3′-UTR, 32% in the 5′-UTR and 23% in the CDS. Comparatively, the distribution of rG4 in the transcriptome is ∼62% 3′-UTR, 16% 5′-UTR, and 20.6% CDS. There does not appear to be a specific consensus sequence, beyond G-richness, for the rG4s found in our candidate protein list, but their abundance in the 5′-UTR is double that of the rG4-seq database. The large enrichment of proteins with rG4-containing mRNA in our list indicates there is good potential for direct regulatory effects to be discovered.

Validating rG4 targets of DDX21

To determine if the change in protein levels observed could be due to altered mRNA abundance, we performed qPCR on RNA extracts from the samples (Fig. 2). While some mRNA levels were found to be significantly different than negative control samples (PSMD11, HNRNPA3, TMPO, CAPZA, HIST1H4A, and CNOT3), there was no significant difference observed between WT and M4 recovery samples, indicating that the altered mRNA levels are likely not due to rG4 activities of DDX21. Since the observed differences between candidate protein levels in WT and M4 samples could not be explained by differences in mRNA abundance, the remaining reasonable explanations are altered translation efficiency or protein stability.

To see if DDX21 preferentially bound to the mRNA of our candidate

FIGURE 1. (*A*) Fold difference in protein levels determined by MS for HEK293T cells expressing M4 DDX21 and WT-DDX21. Two-way Anova tests determined the significance of the difference, error bars represent the standard deviation between three biological replicates. (*B*) Representative western blot showing DDX21 levels for each sample.

proteins we performed immunoprecipitation of DDX21 followed by real-time quantitative PCR (RT-qPCR) on the coprecipitated RNA. Significant enrichment (three standard deviations above GAPDH) of five of the candidate proteins' mRNA was observed (Fig. 3). All five of these mRNAs had previously been shown to have rG4 forming regions, two of which were in their 5′-UTR and three had rG4s in their CDS (Kwok et al. 2016). While each of the five candidates are potentially interesting, we focused our efforts on MAGED2. Our rationale was twofold. First, the MAGED2 rG4 was reportedly in its 5′-UTR (as opposed to the CDS), making it straightforward to introduce mutations to the rG4 forming region to study the impact on translation. Second, the direction of regulation is consistent with the most commonly observed mechanism of rG4 regulation (i.e., steric hindrance by rG4 blocking translation).

Western blots (Fig. 4) with anti-MAGED2 antibodies were performed on the cell lysates used in the mass-spectrometry experiments and confirm the trend observed in Figure 1A. When quantified by densitometry, the western blot data shows that the WT-recovery sample has 1.7 ± 0.2 times the signal observed in the M4-recovery sample, within an error of the 2.00 ± 0.15-fold difference determined by mass-spectrometry. Similarly, there is 2.0 ± 0.2 times as much signal in the negative control sample compared to the DDX21 knockdown sample.

## MAGED2 transcript variant 2 preferentially interacts with DDX21

MAGED2 has three reported transcript variants (TV) that contain different 5′-UTR but have no difference in protein CDS (Fig. 5A). Though the variants share 31 conserved nucleotides before the start codon, their 5′ regions vary in length and sequence; 125 nt for TV1, 234 nt for TV2, and 193 nt for TV3. Bioinformatic analysis
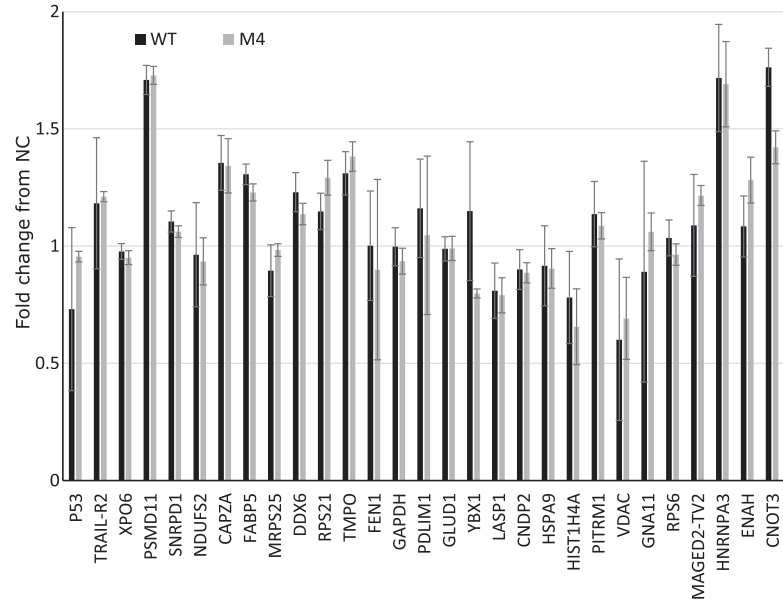
FIGURE 2. RT-qPCR analysis comparing mRNA levels of target proteins between WT and M4 DDX21 recovery samples. Error bars represent the standard deviation between three biological replicates.
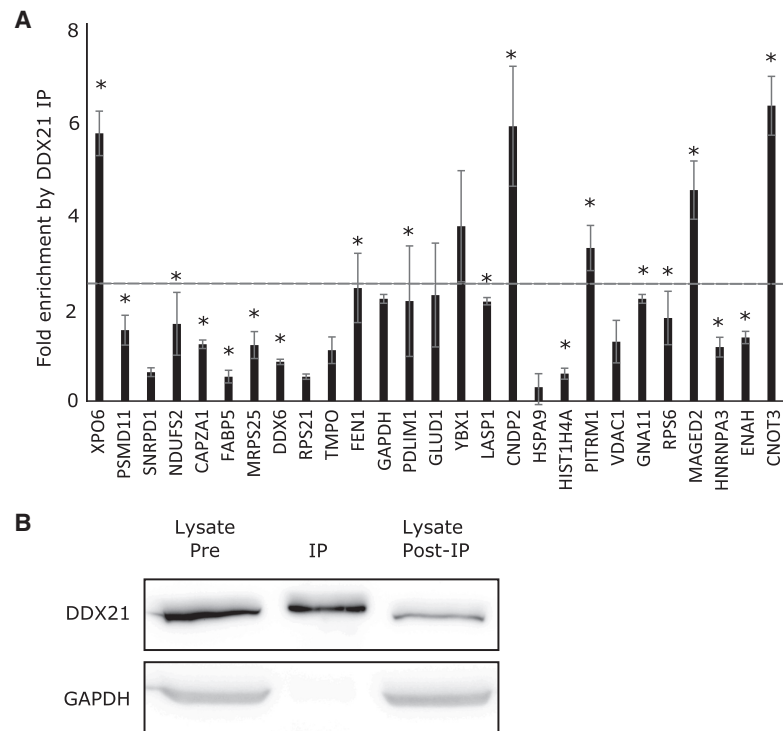
FIGURE 3. (*A*) RIP-qPCR data from HEK293T cell lysate comparing Ct values of DDX21 IP sample to the RNA extracted from the pre-IP lysate. The *horizontal* gray dashed line represents a 3 standard deviation difference in enrichment above GAPDH; error bars represent the standard deviation between three independent IP replicates. (*B*) Western blot showing DDX21 present in the lysate, IP, and to a lesser extent in the post-IP lysate.
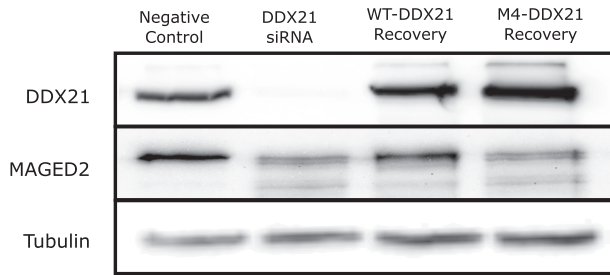
FIGURE 4. Validation of the changes in protein level observed by mass spectrometry between negative control, DDX21 knockdown and WT, or M4-DDX21 recovery samples by western blot. DDX21 knockdown and recovery (*top*) affects the signal from the MAGED2 antibody, but not Tubulin.

of the three transcript variants was performed with the G4RNA web server (Garant et al. 2018) and QGRS mapper (Kikin et al. 2006). This analysis revealed that all transcript variants have rG4 forming potential. The rG4 sequence previously reported for MAGED2 mRNA was from the TV3 5′-UTR (Kwok et al. 2016) and is also predicted to form rG4 by the three software used in our study. The scoring and location of the rG4 forming regions from three rG4 prediction algorithms, QGRS mapper, G4Hunter (Bedrat et al. 2016), and G4RNA screener (Garant et al. 2017) can be found in Figure 5B–D. To decipher which of these transcript variants could be contributing to the regulation of MAGED2 we returned to our DDX21-RNA-IP samples and looked for differences in enrichment between primer sets specific for individual transcript variants (Fig. 5E). While a primer set that does not discriminate between MAGED2 transcript variants is enriched 4.6-fold from pooled cellular RNA, TV1 and TV3 were only enriched 1.7- and 2.2-fold, respectively. TV2 has the highest fold enrichment with a 5.5-fold change, indicating it is preferentially interacting with DDX21 in cell lysate.

In vitro characterization of the MAGED2 transcript variant 2 5′-UTR

To assess the importance of a potential rG4 in the 5′-UTR of the MAGED2 mRNA, a mutant version of TV2 (TV2m) unable to form rG4 was created by mutating all nine runs of consecutive guanines to contain a sin-

gle cytosine that would disrupt each guanine tract (GGG to GCG mutation). The TV2 and TV2m 5′-UTR were in vitro transcribed and purified by size exclusion chromatography. To confirm the possibility of direct interactions with DDX21, electrophoretic mobility shift assays (EMSA) were performed (Fig. 6) with recombinant purified DDX21 and either TV2 and TV2m RNA. At the highest DDX21 concentration (1000 nM) both RNA completely shifted to higher molecular weight complexes, while at the second-highest concentration only the wild-type TV2 was completely shifted. Densitometric analysis using the FluorChem Q software allowed for fitting of the EMSA to a Hill binding model where the recombinant purified DDX21 showed a marginally higher affinity for TV2 versus TV2m (100 nM vs. 300 nM).

Next, TV2 and TV2m were assayed for rG4 formation using ThT, a fluorescent probe sensitive to rG4 formation (De La Faverie et al. 2014; Xu et al. 2016). When ThT is bound to rG4 it exhibits enhanced fluorescence. rG4 conformations are stabilized by K^+ and destabilized by Li^+, while non-rG4 conformations are not greatly affected by these cations (Bhattacharyya et al. 2016). By comparing ThT fluorescence in the presence of rG4 stabilizing and destabilizing cations
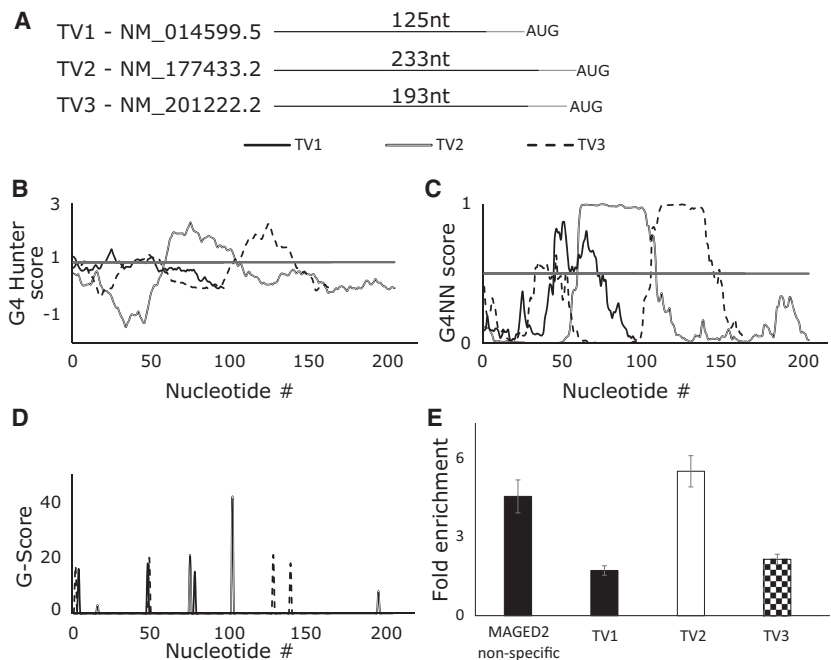
FIGURE 5. (*A*) Graphic depiction of MAGED2 5′-UTR transcript variants 1, 2, and 3 with their accession numbers; the gray ends represent the 31 nt shared by all three transcript variants. (*B–D*) graphic depictions of bioinformatic analysis of MAGED2 5′-UTR transcript variants with G4 Hunter, G4NN, and QGRS mapper, respectively. The prediction was performed using a 30 nt window and a 1nt step size within the G4RNA screener parameters. The horizontal line in *B* and *C* represents the threshold for likely rG4 formation and the nucleotide # refers to the position 5′ most nucleotide involved in the putative rG4. (*E*) DDX21 RNA IP enriches MAGED2 TV2 preferentially to TV1 and TV3 by RT-qPCR. A primer set that detects all MAGED2 transcript variants as well as TV1, TV2, and TV3 specific primer sets were used to determine the enrichment of each transcript variant by DDX21-Immunoprecipitation from pooled cellular RNA.
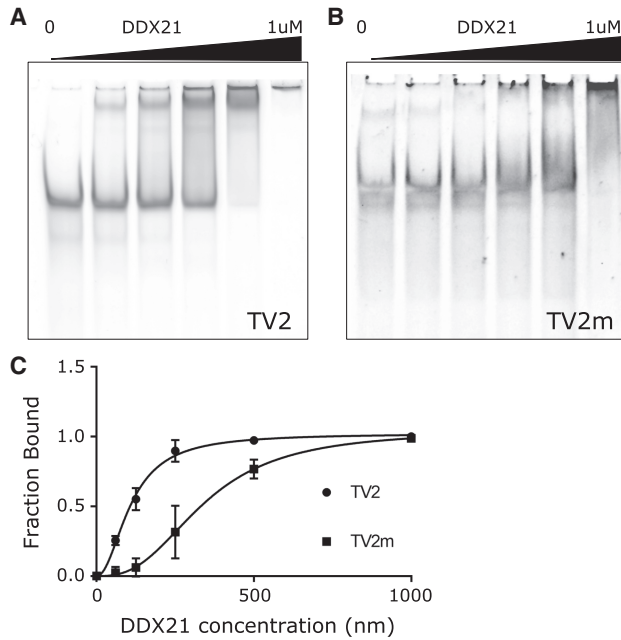
FIGURE 6. Electrophoretic mobility shift assays of MAGED2 5′-UTRs, (A) TV2, (B) TV2m with a serial (1:1) dilution of DDX21. Fitting curves (C) determined in Prism from a Specific binding model with Hill slope from densitometric analysis of EMSA images. Error bars represent the standard deviation between three replicates.

cycle at which the qPCR signal reached its critical threshold Ct was taken as an indicator of the efficiency of cDNA synthesis. To normalize for potential differences in the amount of RNA in the reactions we used a primer set that only covered the 3′ most region of the UTR, before any potential rG4 forming regions. The other primer set spanned the entire RNA. Reverse transcription products that stopped due to structures in the region of mRNA containing the G tracts would not be amplified by the primer set spanning the full UTR, whereas they could still be amplified by the control primer set. For TV2m, both primer sets gave comparable Ct values, resulting in a ΔCt of 0.05 ± 0.48 cycles between them (Fig. 7B). For the wild-type TV2 the Ct was reached 3.06 ± 0.35 cycles later with the primer set spanning the full UTR than the internal control primer set, indicating that a significant number of abortive transcripts were being produced.

Identification of rG4 location and evidence of rG4 unwinding by DDX21

To begin to characterize the rG4 forming sequence in the MAGED2 TV2 UTR we performed reverse transcription reactions on TV2 and TV2m using fluorescently labeled primers; this allowed us to visualize the rt-stop products by
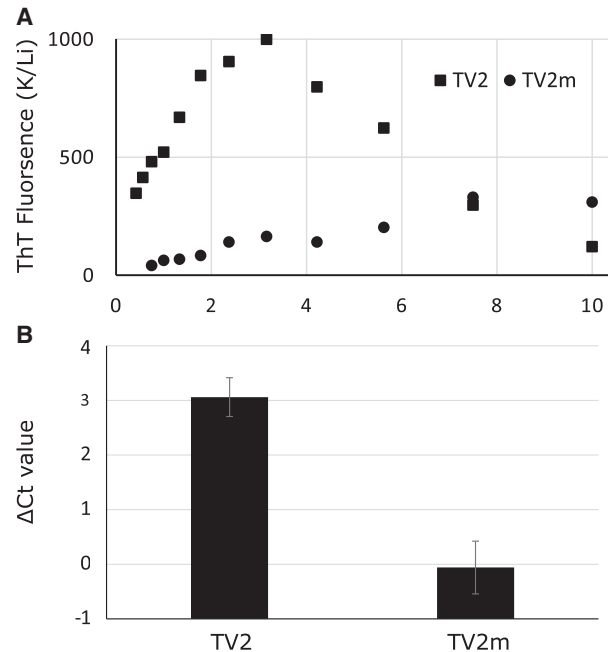
we strengthen the evidence that enhanced fluorescence is due to rG4 formation. TV2 induces significantly more fluorescence from ThT than TV2m, furthermore, the large difference in the fluorescence from the K^+ and Li^+ containing TV2 samples (Fig. 7A) is indicative of rG4 formation being the underlying cause for the fluorescent enhancement by TV2. At lower RNA concentrations TV2 has the greatest difference in ThT fluorescence between K^+ and Li^+ samples but at higher RNA concentrations the difference in fluorescence tapers off, indicating the RNA may be forming rG4 at higher concentrations despite the unfavorable Li^+ cation. TV2m has considerably less effect on ThT fluorescence, typically emitting 10%–30% the amount of fluorescence compared to TV2 at a given concentration; together with a lack of significant difference between TV2m in K^+ or Li^+ containing samples this indicates that TV2m does not form a stable rG4.

Next, we used a modified reverse-transcriptase stop assay (rt-stop) to demonstrate structural differences between TV2 and TV2m. The principle of this assay is that a structured RNA will not be efficiently reverse-transcribed and result in a mixture of full length and aborted transcripts. By comparing the amount of reverse transcriptase stopping between TV2 and TV2m we can infer differences in their 5′-UTR structure. Briefly, reverse transcription reactions were performed on equal amounts of both of the in vitro purified RNA at 37°C for 20 min. After purification of cDNA, qPCR was used to amplify the cDNA and the

FIGURE 7. (A) Thioflavin T fluorescence enhancement on serial dilutions of TV2 and TV2m, the data is presented as the ratio of the normalized fluorescence in K+ versus Li+ containing buffers. (B) Reverse transcriptase stop assay performed on TV2 and TV2m and quantified by qPCR, ΔC_t values represent the difference of the Ct values for the primer set spanning the rG4 forming region and the control primer set. Error bars represent the standard deviation between three reverse transcription reactions.

denaturing PAGE (Fig. 8A). The full length 234 nt cDNA was observed in both TV2 and TV2m reverse transcription reactions, while a shorter ~115 nt cDNA was only observed with TV2 (Fig. 8B). This shorter cDNA is likely the result of a stalled reverse transcriptase that encountered significant secondary structure. From the length of this rt-stop
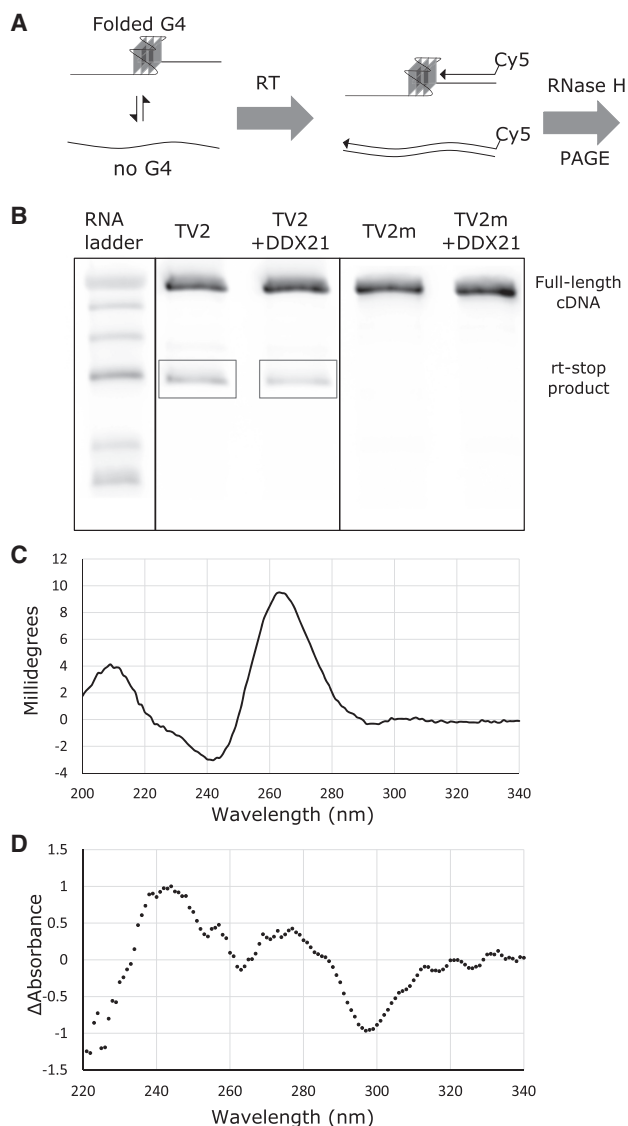
FIGURE 8. (*A*) Cartoon diagram showing the workflow of the rt-stop assay with fluorescent primers. (*B*) Visualization of rt-stop products using fluorescently labeled primers for rt-reactions. The in house prepared RNA ladder (*left*) had 234, 200, 156, 119, 81, and 69 nt Cy5-labeled oligonucleotides. Full-length cDNA products are observed for TV2 and TV2m adjacent to the 234 nt ladder. Reverse transcription-stop products (boxed in gray) are observed only with the TV2 RNA template. Addition of DDX21 (56 nM) to the rt reaction reduces the intensity of the rt-stop by twofold (quantified by densitometry). Template RNA was used at a concentration of 665 nM. (*C*) Circular dichroism spectrum of the 18 nt G4 forming sequence located at the rt-stop location. (*D*) Thermal difference spectrum of the 18 nt G4 forming sequence located at the rt-stop location.

product, we can locate the position of the interfering structure in the TV2 RNA. The rt-stop is immediately prior to a sequence with high rG4 forming potential: (5′GGGCTG GGCTGGGTTGGG3′) nt101–119, as predicted by GQRS mapper, G4Hunter and G4RNA screener (Fig. 5B–D).

When enzymatic amounts of recombinant purified DDX21 is added to the reverse transcription reaction with the TV2 RNA we observe a twofold decrease in rt-stop products by densitometric analysis, remarkably consistent with the change in MAGED2 protein we see with DDX21 knockdown and M4 recovery (Figs. 1A, 3). This data indicates that DDX21 can unwind or destabilize the rG4 within TV2 sufficiently to alter the reverse-transcription efficiency.

While the length of the full 5′-UTR does not allow for a straightforward biophysical characterization, shorter oligonucleotides with a single structural motif are more easily identified. To this end we performed circular dichroism as well as a UV-Vis thermal difference experiment on the 18 nt immediately 5′ of our rt-stop where a putative rG4 may form. A key feature of a parallel rG4 in the circular dichroism spectrum is the nonconservative exciton centred at 250 nm, with a large positive ellipticity at 264 nm and a shallow negative at 240 nm. Further to this, RNA G4 also have positive ellipticity at 210 nm, where A-form RNA are characteristically very negative (Kypr et al. 2009). The thermal difference spectrum is the subtraction of the UV-Vis spectrum of an oligonucleotide in a folded state (20°C) from that of the unfolded state (90°C). The result is a spectroscopic signature that is unique to the oligonucleotide, but allows classification based on its secondary structure. For rG4 the characteristic spectra include a negative peak at 295 nm and two positive peaks around 240 and 280 nm, with a dip in the middle at ~260 nm (Mergny et al. 2005). Using both methods we show that the region of the MAGED2 TV2 5′-UTR that is responsible for the rt-stop can form an rG4 in vitro (Fig. 8C,D).

MAGED2 5′-UTR luciferase assays

TV2 and TV2m were cloned into the dual-luciferase vector, psiCheck-2, immediately 5′ of the *hRLuc* gene such that they would be transcribed as a 5′-UTR. A common criticism of these assays is that the efficient transcription from the promotor on the luciferase vector results in levels of *hRLuc* mRNA that far exceed the levels of mRNA of the endogenous mRNA. In the context of rG4 regulation, the increased number of rG4s could exceed the capacity of the cellular rG4 helicase proteins to unwind them (Serikawa et al. 2017). To mitigate this effect, we truncated the CMV promotor in front of our 5′-UTR to reduce the level of reporter mRNA being made. HEK293T cells were treated as they were for the MS experiments and at 48 h post endogenous DDX21 knockdown they were transfected with the dual-luciferase reporter vector.

In the experiments with the wild-type TV2 5'-UTR, DDX21 knockdown significantly ($P < 0.05$) reduced the luciferase activity from the levels observed in the negative control cells (Fig. 9). This effect was rescued by overexpression of the WT-DDX21 but not M4. In the experiments with TV2m or an empty vector (no 5'-UTR added), no significant change in luciferase activity was detected between NC, KD, WT, or M4 samples.

We also introduced an RNA rG4 stabilizing ligand carboxypyridostatin (Di Antonio et al. 2012) (cPDS) into the luciferase assays to see if there were any rG4 dependent effects on translation. Cells were treated with cPDS immediately prior to transfection of the PsiCheck-2 vector. Compared to the samples that were not treated with cPDS, the treated samples had only 15% of the luciferase activity from the vector with the intact TV2 5'-UTR. The TV2m reporter construct showed no change in luciferase expression in the presence of cPDS. The empty vector samples were similarly unaffected by cPDS with the exception of one replicate having increased luciferase activity, adding significant error to the average luciferase activity.

DDX21 regulates TRAIL-R2 expression and protects cells from TRAIL-mediated apoptosis

MAGED2 has been shown to regulate TRAIL-R2 protein and mRNA levels in a p53-dependent manner (Papageorgio et al. 2007; Tseng et al. 2012; Strekalova et al. 2016). To test whether the changes in MAGED2 level from DDX21 knockdown could affect TRAIL-R2 we performed qPCR on RNA extracted from our knockdown recovery experiments. The RNA from the HEK293T cells showed no difference in mRNA levels of p53, MAGED2 or TRAIL-R2 (Fig. 2). Since this pathway has been shown to be p53-dependent, and HEK293T have p53 suppressed by the SV40 large T antigen (Lin et al. 2014), we repeated
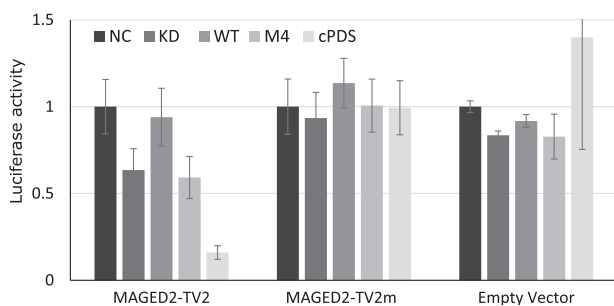
FIGURE 9. The effect of DDX21 status and rG4 stabilizer cPDS on the translation of luciferase mRNA under control of MAGED2 TV2, TV2m, and no 5'-UTRs. Luminescence from the hrLuc protein (under control of the 5'-UTR variant) was normalized to the luminescence from the hLuc protein (consistent 5'-UTR) for each sample and then scaled to the normalized luminescence of the negative control samples of each 5'-UTR variant. Error bars represent the standard deviation between three biological replicates.

the experiment with MCF-7 cells that have wild-type p53 (Leroy et al. 2014). In MCF-7 cells we saw an increase in TRAIL-R2 mRNA levels upon DDX21 knockdown, but not in p53 or MAGED2 mRNA (Fig. 10A). Furthermore, western blots confirm a change in protein levels of TRAIL-R2 in response to DDX21 activity (Fig. 10B). Next, we investigated the TRAIL sensitivity of our four conditions; 72 h after knockdown of DDX21 MCF-7 cells were treated with TRAIL protein and left overnight. To detect TRAIL-mediated apoptosis, we used fluorescent Annexin V to stain cells undergoing apoptosis and counted fluorescent cells by flow cytometry (Fig. 10C). The DDX21 knockdown and M4-DDX21 recovery samples were significantly sensitized to TRAIL-mediated apoptosis with ~20% of the counted cells showed staining by Annexin V. Comparatively the negative control treated cells and the WT-DDX21 recovery had only $0.19 \pm 0.02\%$ and $0.52 \pm 0.18\%$ of cells stained with Annexin V. These results demonstrate that regulation of MAGED2 by DDX21 is enough to affect the TRAIL-sensitization of cells by overexpression of TRAIL-R2.

DISCUSSION

Recently we discovered DDX21 to be an RNA rG4-binding protein that has the ability to destabilize rG4s (McRae et al. 2017). Until now studies have focused on model RNA systems and there are no endogenous rG4s that DDX21 is known to interact with. A unique aspect of our study is the implementation of an RNA helicase protein that has been site-specifically mutated to have reduced affinity for rG4. By comparing differences in the whole-cell proteome in cell populations with either a wild-type or mutant helicase protein we can discern differences that are due to the reduced affinity for rG4. We use this tool to identify, for the first time, biologically relevant rG4 targets of the RNA helicase protein DDX21. This method could also be adapted to the study of other moonlighting proteins where the biochemical data exists to allow for specific mutations that only affect one of its activities.

From the list of proteins affected by replacement of wild-type DDX21 with M4, we validated the effect on MAGED2. A twofold decrease in the MAGED2 protein level is observed by both western blot and mass-spectrometry in cell populations expressing M4 DDX21. MAGED proteins are known to regulate cell cycle progression, apoptosis, and transcription and are up-regulated in key points of embryogenesis as well as in multiple cancer types (Kurt et al. 2000; Barker and Salehi 2002). Overexpression of MAGED2 has been linked to resistance to treatment with TRAIL (Tseng et al. 2012), making it an interesting and valuable target for us to validate for rG4 regulation by DDX21. MAGED2 has been shown to interact with p53 and affect both transcription of and protein levels of TRAIL-R2. It has been hypothesized that increased MAGED2 expression is a mechanism to selectively
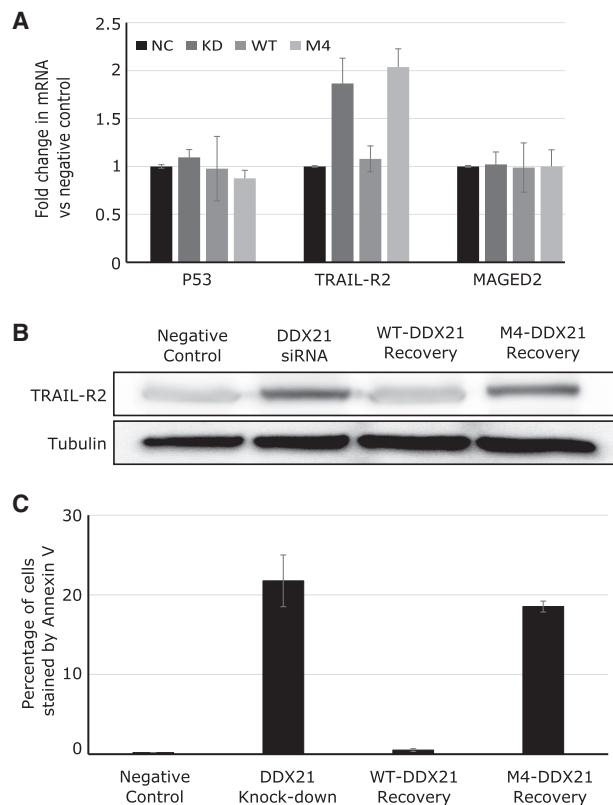
FIGURE 10. Assessing the effects of DDX21 knockdown, WT, and M4 recovery on MCF-7 cells by: (*A*) RT-qPCR for MAGED2 mRNA and its downstream targets TRAIL-R2 and P53. (*B*) Western blot for TRAIL-R2 levels. (*C*) Flow cytometry analysis of Annexin V staining post TRAIL treatment to detect apoptosis. Error bars represent the standard deviation between three biological replicates.

multiple structures existing within the long RNA. Yet no methods exist to deconvolute the individual spectral characteristics of these complex spectra. While other methods such as in-line probing (Beaudoin et al. 2013) can work on longer nucleic acid sequences they do reach a practical limit for separation of the cleavage products after ~100 nt. By using a reverse transcription stopping assay we circumnavigate the length limitations of other rG4 detection methods and examine rG4 formation in the context of the full MAGED2 TV2 5′-UTR. We then incorporated fluorescent primers into the assay estimate the size of the rt-stop product allowing us to approximate the position of the rG4 in the 5′-UTR. When the 18 nt of sequence prior to the stop was analyzed by both circular dichroism and thermal difference spectra, features characteristic of rG4 are observed.

By adding DDX21 into the reverse transcription reaction we turn this easy to perform rG4 detection method into a functional helicase assay. A major downfall of the current methods used to probe rG4 helicase activity is the lack of sequence context surrounding the rG4 structure. In this assay we can convincingly show rG4 disruption in the context of a full length 5′-UTR, in this case, where the rG4 is in the centre of a 234 nt RNA. In our opinion, this is a significant advancement from the trap-based assays (Booy et al. 2015), tetramolecular assays (Creacy et al. 2008), and nuclease sensitivity assays (McRae et al. 2017) used previously. The detection of reverse transcription stops around the G-rich region of TV2 that can be relieved by introduction of DDX21 support the notion of DDX21-affected rG4 formation that can sterically hinder enzyme readthrough, which can be extended to its effect on translation efficiency.

Targeting of rG4 regulated pathways is an emerging area of therapeutic potential for fighting cancer (Rhodes and Lipps 2015; Fay et al. 2018) and sensitization of TRAIL-resistant breast carcinoma to TRAIL-mediated apoptosis is a current therapeutic target (Mérino et al. 2007; Trivedi and Mishra 2015; Manouchehri et al. 2018). Our data underline the potential for the integration of rG4 therapeutics with an existing cancer treatment interest. Current research suggests that DDX21 has a unique specificity for certain rG4s that may be dependent on the loop sequence (McRae et al. 2017, 2018). Further work aims to identify the structure of the TV2 rG4 that DDX21 is recognizing, deciphering the specificity of DDX21 may potentially allow for the design of small molecules that specifically block its action.

MATERIALS AND METHODS

Cell culture and reagents

The HEK293T cell line was a gift from Dr. Thomas Klonisch and the MCF-7 cell line was a gift from Dr. Spencer Gibson. Both cell lines

inactivate certain p53 targets, including TRAIL-R2. Previous studies have shown that a decrease in MAGED2 protein results in up-regulation of p53 and TRAIL-R2 at the mRNA and protein level (Papageorgio et al. 2007; Tseng et al. 2012). We observed a similar effect in MCF-7 cells, revealing a pathway whereby DDX21 can facilitate MAGED2 translation that in turn blocks TRAIL-R2 expression. Replacement of the DDX21 with the M4 mutant results in decreased MAGED2 protein and in turn an increase in TRAIL-R2 expression, indicating that rG4 binding and unwinding is important for efficient translation of MAGED2 mRNA. This increase in TRAIL-R2 expression is significant enough to allow for TRAIL-induced apoptosis in MCF-7 cells depleted of DDX21 or expressing only M4 DDX21.

We determined transcript variant 2 of MAGED2 preferentially interacts with DDX21 and can form rG4 in its 5′-UTR. Due to the length of the 5′-UTR being investigated (234 nt) more traditional rG4 detection methods were not practical. Spectrophotometric methods such as circular dichroism and thermal difference spectroscopy produced complex spectra that are likely a convolution of

were grown in Dulbecco's Modified Eagle Medium from Thermo Fisher Scientific supplemented with 10% Fetal Bovine Serum (Thermo Fisher Scientific). Gibco Trypsin/EDTA solution (Thermo Fisher Scientific) was used to detach the MCF-7 cells. Polyethyleneimine (Thermo Fisher Scientific) was used as the transfection reagent for plasmid DNA transfections.

DDX21 siRNA knockdown and recovery

HEK293T cells were grown to 80% confluence in 150 mm cell culture plates and transfected with empty pcDNA 3.1+ (negative control and knockdown samples) or siRNA resistant wt-DDX21 or m4-DDX21 expressing pcDNA3.1+. The following day the cells were split 1:9 and reverse transfected using transfectamine siRNA Max with either negative control siRNA (negative control sample) or DDX21 siRNA (knockdown and wild-type and m4 recovery samples). Seventy-two hours after reverse transfection the cells were collected in Phosphate Buffered Saline (Thermo Fisher Scientific) and rinsed twice. MCF-7 cells were treated the same way but cultured in six-well dishes and only split 1:3 when reverse transfecting the siRNA. The remainder were lysed in ice-cold RIPA buffer supplemented with 100× HALT proteinase cocktail (Thermo Fisher Scientific). Cells were vortexed and sonicated briefly before pelleting cell debris by centrifugation at 21,000*g*. The protein concentration of the soluble portion was determined by Bradford assay and 50 µg of each sample was used for SDS-PAGE and western blots.

In-gel digestion

Protein lanes were visualized by Coomassie blue staining prior to whole-lane excision. Each lane was subsequently cut into 15 equal bands, with each band corresponding to a region of the gel containing proteins of a distinct molecular weight range. Each of the gel fractions was subjected to in-gel tryptic digestion as previously described (Khan et al. 2015); the resulting extracted peptides were then dried and suspended in 60 µL of 0.2% formic acid in 5% ACN.

LC-MS/MS analysis

Digested peptides were analyzed by LC-MS/MS using a ThermoScientific Easy nLC-1000 in tandem with a Q-Exactive Orbitrap mass spectrometer. Five microliters of each sample was subject to a 120 min gradient (0%–45% buffer B; buffer A: 0.2% formic acid in 5% ACN; buffer B: 0.2% formic acid in ACN) on a 2 cm Acclaim 100 PepMap Nanoviper C18 trapping column in tandem with a New Objective PicoChip reverse-phase analytical LC column. For data-dependent analysis, the top 15 most abundant ions were analyzed for MS/MS analysis while +1 ions were excluded from MS/MS analysis. Additionally, a dynamic exclusion of 10 sec was applied to prevent continued reanalysis of abundant peptides. For the analysis, a resolution of 35,000 was used for full scans that ranged from 400 to 2000 m/z and a resolution of 17,500 was used for MS/MS analysis.

For data analysis, raw data files corresponding to samples comprising an entire gel lane were grouped together and searched using Proteome Discoverer 1.4.1.14's SEQUEST search algorithm

using the reviewed, nonredundant *H. sapien* complete proteome retrieved from UniprotKB. Search parameters were identical to those previously reported (Kramer et al. 2017). During data processing, the "Precursor Ion Area Detector" node of Proteome Discoverer 1.4.1.14's SEQUEST workflow editor was implemented to quantify the extracted ion chromatogram for each protein identified from the raw data. Searched results were filtered using a minimum of two medium confidence peptides per protein.

The mass spectrometry proteomics data have been deposited to the ProteomeXchange Consortium (Deutsch et al. 2017) via the PRIDE (Perez-Riverol et al. 2016, 2019) partner repository with the data set identifier PXD013501.

Protein–RNA coimmunoprecipitation and RT-qPCR

Native RNA immunoprecipitations were performed on one 150 mm dish of HEK293T cells as previously described (Booy et al. 2018) using anti-DDX21 antibody (Novus NB100-1716). RT-qPCR analysis was performed on Applied Biosystems StepOnePlus instrument with the RNA to Ct One-step RT-qPCR kit (Thermo Fisher Scientific) according to the manufacturer's instructions. To determine fold enrichment, RNA was extracted from the total cell lysate using the GeneJET RNA purification kit (Thermo Fisher Scientific) to serve as a reference sample. Twenty-five nanograms of template RNA was used in all RT-qPCR reactions.

Western blots

For each sample, 50 µg of protein in SDS-PAGE load dye was loaded onto a 10% SDS-PAGE gel and ran at a 200V for 45 min. Proteins were transferred to a 0.2 µm PVDF membrane (BioRad Laboratories) using the Trans-Blot Turbo transfer system (BioRad Laboratories). Membranes were blocked for 30 min in 5% milk powder dissolved in Tris Buffered Saline + Tween (TBST) (20 mM Tris pH 7.5, 150 mM NaCl, 0.1% Tween). The following antibodies were used: DDX21 (Novus NB100-1716), MAGED2 (ProteinTech 15252-1-AP), TRAIL-R2 (AbCam EPR19310, AB199357), CNOT3 (ProteinTech 11135-1-AP), XPO6 (ProteinTech 11408-1-AP), GAPDH (Life Technologies AM4300), Mouse anti-Tubulin (T6074, Sigma-Alrich), goat anti-rabbit secondary (Millipore 12–348), goat anti-mouse (Millipore 12–349). DDX21, MAGED2 and TRAIL-R2 primary antibodies were incubated overnight at 4°C in TBST + 5% milk, GAPDH and tubulin primary antibodies were incubated for 1 h at room temperature in TBST + 5% milk. Three sequential 5-min washes with 5% TBS-T were followed by 1-h incubation with secondary antibodies (1:10,000) in TBST + 5% milk and then four more 10-min washes with TBS-T. Prior to imaging with the FluorChem Q system (Protein Simple), 1 mL of Illuminata Forte Western HRP substrate (EMD Millipore) was added to the blots. Due to weak signal from some antibodies a uniform adjustment to the brilliance was made using Inkscape V 0.91.

Annexin V staining and TRAIL treatment

MCF-7 cells were treated as described in the DDX21 siRNA knockdown and recovery section. At 48 h post knockdown, TRAIL protein (Millipore GF092) was added to the media to a final

concentration of 50 ng/mL. Approximately 18 h later the cells were washed with 1× trypsin and then incubated with 1× trypsin at 37°C for 5 min. Detached cells were collected, washed with cold PBS and resuspended in 100 µL of cold 1× Annexin-binding buffer supplemented with AlexaFluor 488 annexin V (Thermo Fisher Scientific) and incubated in the dark for 15 min. Samples were then diluted to 500 µL with 1× Annexin-binding buffer and kept on ice. Annexin V binding was measured using the BD FACSCalibur platform and analyzed using the BD CellQuest Pro software (BD Biosciences), 10,000 cells from each sample were analyzed and each sample performed in biological triplicate.

Cloning

The pcDNA3 vector was used to create a CMV promotor lacking nucleotides between 208 and 746, this was then cloned into the BglII and NheI sites of the psiCHECK-2 vector, removing the SV40 promotor. 5'-UTRs of MAGED2 TV2 and TV3 were amplified by RT-PCR from RNA isolated from human testes tissue purchased from Takara Bio. The 5'-UTR of TV1 was amplified from a DNA fragment purchased from Genscript. Each TV was amplified using primers that contain restriction enzyme sites for NheI and cloned into the psiCHECK-2 vector. The cDNA that encodes the human DDX21 protein, isoform 1, was amplified by PCR using DNA primers that were designed to encode a NheI and NotI restriction enzyme sites and cloned into the pET28b expression vector.

Luciferase assays

For luciferase assays, HEK293T cells were treated as described in the DDX21 siRNA knockdown and recovery section scaled down to a six-well dish sample size. Forty-eight hours post knockdown, the cells were transfected with 1 µg of psiCheck-2 vector in 250 µL serum-free DMEM with 1.5 µg of polyethyleneimine. For carboxypyridostatin treated cells, cPDS was added to a concentration of 1 µM immediately prior to the transfection of the psiCheck-2 vector. Twenty-four hours after the transfection of Psi-Check-2, the cells were collected in cold PBS. Half of the cells were used for RNA purification using the GeneJET RNA purification kit (Thermo Fisher Scientific) and the other half used in the luciferase assay. The Dual-Glo Luciferase Assay system (Promega) was used according to manufacturer instructions, luminescence was measured for 10 sec using the SpectraMax iD3 plate reader and each sample performed in at least biological triplicate. To control for transfection efficiency and sample preparation, luminescence from the hRluc protein, under control of the 5'-UTR of interest was normalized to the signal from the hluc protein from the same sample. The normalized luminescence from the negative control sample was then set to 1 and the other conditions scaled accordingly.

In vitro transcription and protein purification

The 5'-UTRs of each transcript variant were transcribed and purified in vitro as previously described (Booy et al. 2012) from linearized recombinant psiCHECK2 vector (Promega) that contained one of the three UTR sequences downstream from a T7 promoter. The vector was linearized with NcoI restriction enzyme and purified by phenol–chloroform extraction. In vitro transcription was carried out at 37°C for 3 h. The transcription reaction was then stopped by addition of EDTA and T7 polymerase was removed by phenol–chloroform extraction. Residual phenol was removed using a DG10 desalting column (BioRad), from which the RNA was eluted in 20 mM Tris pH 7.5, 1 mM EDTA and either 100 mM KCl (TEK), or 100 mM LiCl (TELi). The RNA was then separated from the plasmid and remaining NTPs by FPLC purification using a Superdex 200 filtration column (GE Healthcare Life Sciences) using TEK or TELi buffer. FPLC fractions were then concentrated and stored at 4°C. RNAs were heated at 95°C and cooled on ice prior to use.

DDX21 was purified from LOBSTR *E. coli* BL21 (DE3) (Kerafast Inc.) cells transformed with DDX21 expressing pET28b. The stop codon from *DDX21* cDNA was retained so that the recombinant protein only had the amino-terminal 6His tag and thrombin cleavage site and not the carboxy-terminal 6×His-tag. Cells were grown at 37°C in a shaker incubator to an optical density of 0.4 at A_{600}, then induced with 0.3 mM IPTG and grown overnight at 18°C. Cells were pelleted, then resuspended in 20 mM Tris 7.5, 1 M NaCl, 10% glycerol, 1 mM DTT and 1 mM PMSF, and lysed by sonication. After centrifugation of lysate, recombinant DDX21 was purified from the soluble fraction using HisPur Cobalt Resin (Thermo-Fisher) and eluted using 200 mM imidazole. Elution fractions were dialyzed against 20 mM Tris pH 7.5, 300 mM NaCl, 10% glycerol, 2 mM DTT, and stored at 4°C.

Electrophoretic mobility shift assays

DDX21, or an equal volume of protein storage buffer (20 mM Tris pH 7.5, 300 mM NaCl, 10% glycerol, 2 mM DTT) was added to the binding reactions in a 1:1 serial dilution, with the first condition containing no DDX21. Binding reactions were performed with 100 nM RNA in 50 mM Tris-acetate, pH 7.8, 100 mM KCl, 10 mM NaCl, 3 mM $MgCl_2$, 70 mM glycine, 10% glycerol, 0.05 mg/mL bovine serum albumin (BSA) for 10 min at room temperature and resolved by native Tris-borate EDTA (TBE) 8% polyacrylamide gel electrophoresis (TBE-PAGE) for 150 min at 75 V. The RNAs were then stained with the fluorescent nucleic acid dye SYBR Gold and imaged on a Fluorchem Q imaging system using the Cy2 excitation LEDs and emission filters (Protein Simple).

Thioflavin T assays

In a 96-well plate, the in vitro transcribed RNA was serially diluted 3:1 with 20 mM Tris pH 7.5, 1 mM EDTA and either 100mM KCl or 100 mM LiCl, from 10 to 0.4 µM. Thioflavin T was added with a final concentration of 1.5 µM. Samples incubated for 5 min at room temperature and fluorescence was measured with Applied Biosystems Step-One-Plus qPCR machine. Fluorescence data was extracted from the BLUE channel from the raw data output of the Step-One-Plus.

Reverse transcriptase stop assays

First-strand synthesis of cDNA from 50 ng of in vitro transcribed 5'-UTR of TV2 and TV2m was performed in a 20 µL reaction using 1 µM reverse primer, 500 µM dNTPs, 4 µL 5× RT Buffer (250 mM Tris-HCl [pH 8.3 at 25°C], 375 mM KCl, 15 mM MgCl2, 50 mM

DTT) (Thermo Fisher), and 200U Maxima H-Minus RT (Thermo-Fisher). Reactions were carried out at 37°C for 60 min before heating at 85°C for 5 min to inactivate the RT enzyme. The cDNA was diluted 1:20 to the qPCR reaction using PowerUp Sybr Green Master Mix (Applied Biosystems), forward primers were added to a final concentration of 1 µM. Forty cycles of qPCR were performed with 60°C annealing temperature and 30 sec extension time using a Step-One-Plus qPCR machine (Applied Biosystems). CT values were determined using StepOne software.

For visualization of rt-stop products, first-strand synthesis of cDNA from 1 µg of in vitro transcribed TV2 and TV2m was performed in a 20 µL reaction using 1 µM Cy5 labeled primer, 500 µM dNTPs, 4 µL 5× RT Buffer (250 mM Tris-HCl [pH 8.3 at 25°C], 375 mM KCl, 15 mM MgCl2, 50 mM DTT) (Thermo Fisher), and 200U Maxima H-Minus RT (Thermo-Fisher). Reactions were performed at 37°C, with or without 56 nM DDX21, for 60 min before heating at 85°C for 5 min to inactivate the RT. To remove DNA:RNA heteroduplex from the reactions, the cDNA samples were treated with RNase H for 20 min at 37°C. After RNase H digestion, cDNA was mixed with an equal volume of denaturing RNA load dye (95% formamide, 0.01% SDS, 0.5 mM EDTA, 0.025% [w/v] Orange G), heated at 95°C for 5 min, and resolved by TBE-urea PAGE with 12% acrylamide gels. Cy5 labeled RNA ladder was prepared as described previously (Booy et al. 2016) with the addition of Cy5-labeled TV2 for the additional 234 nt band. Reverse transcription products and ladder were visualized with Cy5 excitation and emission filters.

Circular dichroism

Circular dichroism spectra were recorded at room temperature using a Jasco J-810 spectropolarimeter (Jasco Inc.) using scanning mode, with a 1 nm data pitch, 50 nm/min scanning speed and a 1 sec response time. A total of 10 µM RNA in TEK in a 0.1 cm quartz cell (Hellma) was measured six times and the data averaged and background subtracted with a buffer spectrum.

Thermal difference spectra

RNA was measured at a concentration of 5 µM in TEK buffer. UV-Vis spectra were collected using a temperature-controlled Evolution 260 Bio UV-Vis spectrophotometer (Thermo Scientific) from 340 to 220 nm at 20°C and 90°C. The 20°C spectrum was then subtracted from the 90° spectrum and then normalized to the wavelength with the highest difference.

SUPPLEMENTAL MATERIAL

Supplemental material is available for this article.

ACKNOWLEDGMENTS

REFERENCES

Barker PA, Salehi A. 2002. The MAGE proteins: emerging roles in cell cycle progression, apoptosis, and neurogenetic disease. *J Neurosci Res* **67:** 705–712. doi:10.1002/jnr.10160

Beaudoin JD, Jodoin R, Perreault JP. 2013. In-line probing of RNA G-quadruplexes. *Methods* **64:** 79–87. doi:10.1016/j.ymeth.2013.02.017

Bedrat A, Lacroix L, Mergny JL. 2016. Re-evaluation of G-quadruplex propensity with G4Hunter. *Nucleic Acids Res* **44:** 1746–1759. doi:10.1093/nar/gkw006

Bhattacharyya D, Mirihana Arachchilage G, Basu S. 2016. Metal cations in G-quadruplex folding and stability. *Front Chem* **4:** 38. doi:10.3389/fchem.2016.00038

Bolduc F, Garant JM, Allard F, Perreault JP. 2016. Irregular G-quadruplexes found in the untranslated regions of human mRNAs influence translation. *J Biol Chem* **291:** 21751–21760. doi:10.1074/jbc.M116.744839

Booy EP, Meng H, McKenna SA. 2012. Native RNA purification by gel filtration chromatography. *Methods Mol Biol* **941:** 69–81. doi:10.1007/978-1-62703-113-4_6

Booy EP, Howard R, Marushchak O, Ariyo EO, Meier M, Novakowski SK, Deo SR, Dzananovic E, Stetefeld J, McKenna SA. 2014. The RNA helicase RHAU (DHX36) suppresses expression of the transcription factor PITX1. *Nucleic Acids Res* **42:** 3346–3361. doi:10.1093/nar/gkt1340

Booy EP, McRae EKS, McKenna SA. 2015. Biochemical characterization of G4 quadruplex telomerase RNA unwinding by the RNA helicase RHAU. *Methods Mol Biol* **1259:** 125–135. doi:10.1007/978-1-4939-2214-7_9

Booy EP, McRae EKS, Howard R, Deo SR, Ariyo EO, Dzananovic E, Meier M, Stetefeld J, McKenna SA. 2016. RNA helicase associated with AU-rich element (RHAU/DHX36) interacts with the 3′-tail of the long non-coding RNA BC200 (BCYRN1). *J Biol Chem* **291:** 5355–5372. doi:10.1074/jbc.M115.711499

Booy EP, McRae EKS, Ezzati P, Choi T, Gussakovsky D, McKenna SA. 2018. Comprehensive analysis of the BC200 ribonucleoprotein reveals a reciprocal regulatory function with CSDE1/UNR. *Nucleic Acids Res* **46:** 11575–11591. doi:10.1093/nar/gkx860

Bugaut A, Balasubramanian S. 2012. 5′-UTR RNA G-quadruplexes: translation regulation and targeting. *Nucleic Acids Res* **40:** 4727–4741. doi:10.1093/nar/gks068

Calo E, Flynn RA, Martin L, Spitale RC, Chang HY, Wysocka J. 2014. RNA helicase DDX21 coordinates transcription and ribosomal RNA processing. *Nature* **518:** 249–253. doi:10.1038/nature13923

Calo E, Gu B, Bowen ME, Aryan F, Zalc A, Liang J, Flynn RA, Swigut T, Chang HY, Attardi LD, et al. 2018. Tissue-selective effects of nucleolar stress and rDNA damage in developmental disorders. *Nature* **554:** 112–117. doi:10.1038/nature25449

Chen G, Liu C-H, Zhou L, Krug RM. 2014. Cellular DDX21 RNA helicase inhibits influenza A virus replication but is counteracted by the viral NS1 protein. *Cell Host Microbe* **15:** 484–493. doi:10.1016/j.chom.2014.03.002

Chen MC, Tippana R, Demeshkina NA, Murat P, Balasubramanian S, Myong S, Amaré ARF. 2018. Structural basis of G-quadruplex

unfolding by the DEAH/RHA helicase DHX36. *Nature* **558:** 465–469. doi:10.1038/s41586-018-0209-9

Cimino D, Fuso L, Sfiligoi C, Biglia N, Ponzone R, Maggiorotto F, Russo G, Cicatiello L, Weisz A, Taverna D, et al. 2008. Identification of new genes associated with breast cancer progression by gene expression analysis of predefined sets of neoplastic tissues. *Int J Cancer* **123:** 1327–1338. doi:10.1002/ijc.23660

Creacy SD, Routh ED, Iwamoto F, Nagamine Y, Akman SA, Vaughn JP. 2008. G4 resolvase 1 binds both DNA and RNA tetramolecular quadruplex with high affinity and is the major source of tetramolecular quadruplex G4-DNA and G4-RNA resolving activity in HeLa cell lysates. *J Biol Chem* **283:** 34626–34634. doi:10.1074/jbc.M806277200

De La Faverie AR, Guédin A, Bedrat A, Yatsunyk LA, Mergny JL. 2014. Thioflavin T as a fluorescence light-up probe for G4 formation. *Nucleic Acids Res* **42:** e65. doi:10.1093/nar/gku111

Deutsch EW, Csordas A, Sun Z, Jarnuczak A, Perez-Riverol Y, Ternent T, Campbell DS, Bernal-Llinares M, Okuda S, Kawano S, et al. 2017. The ProteomeXchange consortium in 2017: supporting the cultural change in proteomics public data deposition. *Nucleic Acids Res* **45:** D1100–D1106. doi:10.1093/nar/gkw936

Di Antonio M, Biffi G, Mariani A, Raiber EA, Rodriguez R, Balasubramanian S. 2012. Selective RNA versus DNA G-quadruplex targeting by situ click chemistry. *Angew Chem Int Ed Engl* **51:** 11073–11078. doi:10.1002/anie.201206281

Dong Y, Ye W, Yang J, Han P, Wang Y, Ye C, Weng D, Zhang F, Xu Z, Lei Y. 2016. DDX21 translocates from nucleus to cytoplasm and stimulates the innate immune response due to dengue virus infection. *Biochem Biophys Res Commun* **473:** 648–653. doi:10.1016/j.bbrc.2016.03.120

Fay MM, Lyons SM, Ivanov P. 2018. RNA G-quadruplexes in biology: principles and molecular mechanisms. *J Mol Biol* **429:** 2127–2147.

Garant JM, Perreault JP, Scott MS. 2017. Motif independent identification of potential RNA G-quadruplexes by G4RNA screener. *Bioinformatics* **33:** 3532–3537. doi:10.1093/bioinformatics/btx498

Garant JM, Perreault JP, Scott MS. 2018. G4RNA screener web server: user focused interface for RNA G-quadruplex prediction. *Biochimie* **151:** 115–118. doi:10.1016/j.biochi.2018.06.002

Hammond JA, Zhou L, Lamichhane R, Chu H-Y, Millar DP, Gerace L, Williamson JR. 2018. A survey of DDX21 activity during Rev/RRE complex formation. *J Mol Biol* **430:** 537–553. doi:10.1016/j.jmb.2017.06.023

Henning D, So RB, Jin R, Lau LF, Valdez BC. 2003. Silencing of RNA helicase II/Guα inhibits mammalian ribosomal RNA production. *J Biol Chem* **278:** 52307–52314. doi:10.1074/jbc.M310846200

Holmström TH, Mialon A, Kallio M, Nymalm Y, Mannermaa L, Holm T, Johansson H, Black E, Gillespie D, Salminen TA, et al. 2008. . c-Jun supports ribosomal RNA processing and nucleolar localization of RNA helicase DDX21. *J Biol Chem* **283:** 7046–7053. doi:10.1074/jbc.M709613200

Huang H, Zhang J, Harvey SE, Hu X, Cheng C. 2017. RNA G-quadruplex secondary structure promotes alternative splicing via the RNA-binding protein hnRNPF. *Genes Dev* **31:** 2296–2309. doi:10.1101/gad.305862.117

Jung Y, Lee S, Choi H-S, Kim S-N, Lee E, Shin Y, Seo J, Kim B, Jung Y, Kim WK, et al. 2011. Clinical validation of colorectal cancer biomarkers identified from bioinformatics analysis of public expression data. *Clin Cancer Res* **17:** 700–709. doi:10.1158/1078-0432.CCR-10-1300

Khan SR, Baghdasarian A, Nagar PH, Fahlman R, Jurasz P, Michail K, Aljuhani N, Siraki AG. 2015. Proteomic profile of aminoglutethimide-induced apoptosis in HL-60 cells: role of myeloperoxidase and arylamine free radicals. *Chem Biol Interact* **239:** 129–138. doi:10.1016/j.cbi.2015.06.020

Kikin O, D'Antonio L, Bagga PS. 2006. QGRS Mapper: a web-based server for predicting G-quadruplexes in nucleotide sequences. *Nucleic Acids Res* **34:** 676–682. doi:10.1093/nar/gkl253

Kramer DA, Eldeeb MA, Wuest M, Mercer J, Fahlman RP. 2017. Proteomic characterization of EL4 lymphoma-derived tumors upon chemotherapy treatment reveals potential roles for lysosomes and caspase-6 during tumor cell death in vivo. *Proteomics* **17:** 1–11. doi:10.1002/pmic.201700060

Kurt RA, Urba WJ, Schoof DD. 2000. Isolation of genes overexpressed in freshly isolated breast cancer specimens. *Breast Cancer Res Treat* **59:** 41–48. doi:10.1023/A:1006315919985

Kwok CK, Marsico G, Sahakyan AB, Chambers VS, Balasubramanian S. 2016. rG4-seq reveals widespread formation of G-quadruplex structures in the human transcriptome. *Nat Methods* **13:** 841–844. doi:10.1038/nmeth.3965

Kypr J, Kejnovská I, Renčiuk D, Vorlíčková M. 2009. Circular dichroism and conformational polymorphism of DNA. *Nucleic Acids Res* **37:** 1713–1725. doi:10.1093/nar/gkp026

Leroy B, Girard L, Hollestelle A, Minna JD, Gazdar AF, Soussi T, Medical S. 2014. Analysis of TP53 mutation status in human cancer cell lines: a reassessment. *Hum Mutat* **35:** 756–765. doi:10.1002/humu.22556

Lin Y, Boone M, Meuris L, Lemmens I, Van Roy N, Soete A, Drmanac R, Chen J, Reumers J, Moisse M, et al. 2014. Genome dynamics of the human embryonic kidney 293 lineage in response to cell biology manipulations. *Nat Commun* **5:** 4767. doi:10.1038/ncomms5767

Lucas S, Brasseur F, Boon T. 1999. A new MAGE gene with ubiquitous expression does not code for known MAGE antigens recognized by T cells. *Cancer Res* **59:** 4100–4103.

Manouchehri JM, Turner KA, Kalafatis M. 2018. TRAIL-induced apoptosis in TRAIL-resistant breast carcinoma through quercetin cotreatment. *Breast Cancer* **12:** 1–12. doi:10.1177/1178223417749855

McRae EKS, Booy EP, Moya-Torres A, Ezzati P, Stetefeld J, McKenna SA. 2017. Human DDX21 binds and unwinds RNA guanine quadruplexes. *Nucleic Acids Res* **45:** 6656–6668. doi:10.1093/nar/gkx380

McRae EKS, Davidson DE, Dupas SJ, McKenna SA. 2018. Insights into the RNA quadruplex binding specificity of DDX21. *Biochim Biophys Acta* **1862:** 1973–1979. doi:10.1016/j.bbagen.2018.06.009

Mergny JL, Li J, Lacroix L, Amrane S, Chaires JB. 2005. Thermal difference spectra: a specific signature for nucleic acid structures. *Nucleic Acids Res* **33:** e138. doi:10.1093/nar/gni134

Mérino D, Lalaoui N, Morizot A, Solary E, Micheau O. 2007. TRAIL in cancer therapy: present and future challenges. *Expert Opin Ther Targets* **11:** 1299–1314. doi:10.1517/14728222.11.10.1299

Morris MJ, Negishi Y, Pazsint C. 2010. An RNA G-Quadruplex is essential for cap-independent translation initiation in human VEGF IRES. *J Am Chem Soc* **132:** 17831–17839. doi:10.1021/ja106287x

Murat P, Marsico G, Herdy B, Ghanbarian A, Portella G, Balasubramanian S. 2018. RNA G-quadruplexes at upstream open reading frames cause DHX36- and DHX9-dependent translation of human mRNAs. *Genome Biol* **19:** 229. doi:10.1186/s13059-018-1602-2

Papageorgio C, Brachmann R, Zeng J, Culverhouse R, Zhang W, McLeod H. 2007. MAGED2 : a novel p53-dissociator. *Int J Oncol* **31:** 1205–1211.

Perez-Riverol Y, Xu Q-W, Wang R, Uszkoreit J, Griss J, Sanchez A, Reisinger F, Csordas A, Ternent T, del-Toro N, et al. 2016. PRIDE inspector toolsuite: moving toward a universal visualization tool for proteomics data standard formats and quality assessment of proteomeXchange datasets. *Mol Cell Proteomics* **15:** 305–317. doi:10.1074/mcp.O115.050229

Perez-Riverol Y, Csordas A, Bai J, Bernal-Llinares M, Hewapathirana S, Kundu DJ, Inuganti A, Griss J, Mayer G, Eisenacher M, et al. 2019. The PRIDE database and related tools and resources in 2019: improving support for quantification data. *Nucleic Acids Res* **47:** D442–D450. doi:10.1093/nar/gky1106

Rhodes D, Lipps HJ. 2015. Survey and summary G-quadruplexes and their regulatory roles in biology. *Nucleic Acids Res* **43:** 8627–8637. doi:10.1093/nar/gkv862

Ribeiro MM, Teixeira GS, Martins L, Marques MR, de Souza AP, Line SRP. 2014. G-quadruplex formation enhances splicing efficiency of PAX9 intron 1. *Hum Genet* **134:** 37–44. doi:10.1007/s00439-014-1485-6

Rogers GW, Edelman GM, Mauro VP. 2004. Differential utilization of upstream AUGs in the -secretase mRNA suggests that a shunting mechanism regulates translation. *Proc Natl Acad Sci* **101:** 2794–2799. doi:10.1073/pnas.0308576101

Rouleau S, Glouzon JPS, Brumwell A, Bisaillon M, Perreault JP. 2017. 3′ UTR G-quadruplexes regulate miRNA binding. *RNA* **23:** 1172–1179. doi:10.1261/rna.060962.117

Sauer M, Juranek SA, Marks J, De Magis A, Kazemier HG, Hilbig D, Benhalevy D, Wang X, Hafner M, Paeschke K. 2019. DHX36 prevents the accumulation of translationally inactive mRNAs with G4-structures in untranslated regions. *Nat Commun* **10:** 2421. doi:10.1038/s41467-019-10432-5

Serikawa T, Eberle J, Kurreck J. 2017. Effects of genomic disruption of a guanine quadruplex in the 5′ UTR of the Bcl-2 mRNA in melanoma cells. *FEBS Lett* **591:** 3649–3659. doi:10.1002/1873-3468.12855

Sloan KE, Leisegang MS, Doebele C, Ramírez AS, Simm S, Safferthal C, Kretschmer J, Schorge T, Markoutsa S, Haag S, et al. 2015. The association of late-acting snoRNPs with human pre-ribosomal complexes requires the RNA helicase DDX21. *Nucleic Acids Res* **43:** 553–564. doi:10.1093/nar/gku1291

Strekalova E, Malin D, Good DM, Cryns VL. 2016. Methionine deprivation induces a targetable vulnerability in triple-negative breast cancer cells by enhancing TRAIL receptor-2 expression. *Clin Cancer Res* **21:** 2780–2791. doi:10.1158/1078-0432.CCR-14-2792

Trivedi R, Mishra DP. 2015. Trailing TRAIL resistance : novel targets for TRAIL sensitization in cancer cells. *Front Oncol* **5:** 69. doi:10.3389/fonc.2015.00069

Tseng HY, Chen LH, Ye Y, Tay KH, Jiang CC, Guo ST, Jin L, Hersey P, Zhang XD. 2012. The melanoma-associated antigen MAGE-D2 suppresses TRAIL receptor 2 and protects against TRAIL-induced apoptosis in human melanoma cells. *Carcinogenesis* **33:** 1871–1881. doi:10.1093/carcin/bgs236

Valdez BC. 2000. Structural domains involved in the RNA folding activity of RNA helicase II/Gu protein. *Eur J Biochem* **267:** 6395–6402. doi:10.1046/j.1432-1327.2000.01727.x

Valdez BC, Henning D, Perumal K, Busch H. 1997. RNA-unwinding and RNA-folding activities of RNA helicase II/Gu–two activities in separate domains of the same protein. *Eur J Biochem* **250:** 800–807. doi:10.1111/j.1432-1033.1997.00800.x

Weldon C, Dacanay JG, Gokhale V, Boddupally PVL, Behm-Ansmant I, Burley GA, Branlant C, Hurley LH, Dominguez C, Eperon IC. 2018. Specific G-quadruplex ligands modulate the alternative splicing of Bcl-X. *Nucleic Acids Res* **46:** 886–896. doi:10.1093/nar/gkx1122

Xiao J, Chen HS. 2005. Biological functions of melanoma-associated antigens (MAGEs) in cell activities. *World J Gastroenterol* **10:** 1849–1853. doi:10.3748/wjg.v10.i13.1849

Xu S, Li Q, Xiang J, Yang Q, Sun H, Guan A, Wang L, Liu Y, Yu L, Shi Y, et al. 2016. Thioflavin T as an efficient fluorescence sensor for selective recognition of RNA G-quadruplexes. *Sci Rep* **6:** 24793. doi:10.1038/srep24793

Yang H, Zhou J, Ochs RL, Henning D, Jin R, Valdez BC. 2003. Downregulation of RNA helicase II/Gu results in the depletion of 18 and 28 S rRNAs in *Xenopus* oocyte. *J Biol Chem* **278:** 38847–38859. doi:10.1074/jbc.M302258200

Zhang Y, Zhang B. 2008. TRAIL resistance of breast cancer cells is associated with constitutive endocytosis of death receptors 4 and 5. *Mol Cancer Res* **6:** 1861–1872. doi:10.1158/1541-7786.MCR-08-0313

Zhang Z, Kim T, Bao M, Facchinetti V, Jung SY, Ghaffari AA, Qin J, Cheng G, Liu Y-J. 2011. DDX1, DDX21, and DHX36 helicases form a complex with the adaptor molecule TRIF to sense dsRNA in dendritic cells. *Immunity* **34:** 866–878. doi:10.1016/j.immuni.2011.03.027

Zhang Y, Baysac KC, Yee L-F, Saporita AJ, Weber JD. 2014. Elevated DDX21 regulates c-Jun activity and rRNA processing in human breast cancers. *Breast Cancer Res* **16:** 449. doi:10.1186/s13058-014-0449-z

Zhang H, Zhang Y, Chen C, Zhu X, Zhang C, Xia Y, Zhao Y, Andrisani OM, Kong L. 2018. A double-negative feedback loop between DEAD-box protein DDX21 and Snail regulates epithelial-mesenchymal transition and metastasis in breast cancer. *Cancer Lett* **437:** 67–78. doi:10.1016/j.canlet.2018.08.021